Check for updates

ADVANCED FUNCTIONAL MATERIALS
www.afm-journal.de

Laser-Induced Real-Space Topology Control of Spin Wave Resonances

Tim Titze, Sabri Koraltan, Timo Schmidt, Marcel Möller, Florian Bruckner, Claas Abert, Dieter Suess, Claus Ropers, Daniel Steil, Manfred Albrecht, and Stefan Mathias**

Femtosecond laser excitation of materials exhibiting magnetic spin textures promises advanced magnetic control via the generation of non-equilibrium spin dynamics. Ferrimagnetic [Fe(0.35 nm)/Gd(0.40 nm)]$_{160}$ multilayers are used to explore this approach, as they host a rich diversity of magnetic textures from stripe domains at low magnetic fields, a dense bubble/skyrmion lattice at intermediate fields, and a single domain state for high magnetic fields. Using femtosecond magneto-optics, distinct coherent spin wave dynamics are observed in this material in response to a weak laser excitation, enabling an unambiguous identification of the different magnetic spin textures. Moreover, employing strong laser excitation, versatile control of the coherent spin dynamics via non-equilibrium transformation of magnetic spin textures becomes possible by both creating and annihilating bubbles/skyrmions. Micromagnetic simulations and Lorentz transmission electron microscopy with in situ optical excitation corroborate these findings.

1. Introduction

Magnetic spin textures are expected to be an important building block for future spintronic- and magnonic-based memory and logic devices, and even for unconventional computing techniques such as neuromorphic computing.[1–7] Especially, localized magnetic solitons, known as skyrmions, have attracted significant attention to be utilized in spin texture based devices.[8–10] Potential applications of magnetic textures include the engineering of spin wave dispersions in magnonic crystals, using magnetic textures as spin wave phase shifters in logic devices, and employing them as nanoscale spin wave emitters to name a few.[11–13] Obviously, the ability to actively control such devices by non-destructive and fast means is highly desirable from an application point of view. Laser-induced manipulation of spin textures is a potential avenue to achieve these goals. However, optical spectroscopy studies in spin-textured material systems have so far either focused on precessional spin dynamics present in low-temperature skyrmionic phases,[14–17] or on statically observed laser-induced transformations of spin textures.[18–21] Here, we show that we can achieve optical control of spin textures at room temperature and thus laser-induced tuning of spin wave resonances to specific frequency ranges. Our work opens new avenues for future actively controlled magnetic spin texture-based devices.

2. Results

2.1. Static Magnetic Properties of [Fe(0.35 nm)/Gd(0.40 nm)]$_{160}$ Thin Films

The sample system we investigated using the time-resolved magneto-optical Kerr effect (TR-MOKE) is a multilayer stack of

T. Titze, D. Steil, S. Mathias
University of Göttingen, I. Physikalisches Institut
37077 Göttingen, Germany
E-mail: dsteil@gwdg.de; smathias@uni-goettingen.de
S. Koraltan, F. Bruckner, C. Abert, D. Suess
Physics of Functional Materials
Faculty of Physics
University of Vienna
Vienna 1090, Austria
S. Koraltan
Vienna Doctoral School in Physics
University of Vienna
Vienna 1090, Austria
The ORCID identification number(s) for the author(s) of this article can be found under https://doi.org/10.1002/adfm.202313619

© 2024 The Authors. Advanced Functional Materials published by Wiley-VCH GmbH. This is an open access article under the terms of the Creative Commons Attribution License, which permits use, distribution and reproduction in any medium, provided the original work is properly cited.

DOI: 10.1002/adfm.202313619

T. Schmidt, M. Albrecht
Institute of Physics
University of Augsburg
86135 Augsburg, Germany
M. Möller, C. Ropers
University of Göttingen, IV. Physikalisches Institut
37077 Göttingen, Germany
M. Möller, C. Ropers
Max Planck Institute for Multidisciplinary Sciences
37077 Göttingen, Germany
C. Abert, D. Suess
Research Platform MMM Mathematics-Magnetism-Materials
University of Vienna
Vienna 1090, Austria
C. Ropers, S. Mathias
University of Göttingen, International Center for Advanced Studies of Energy Conversion (ICASEC)
37077 Göttingen, Germany

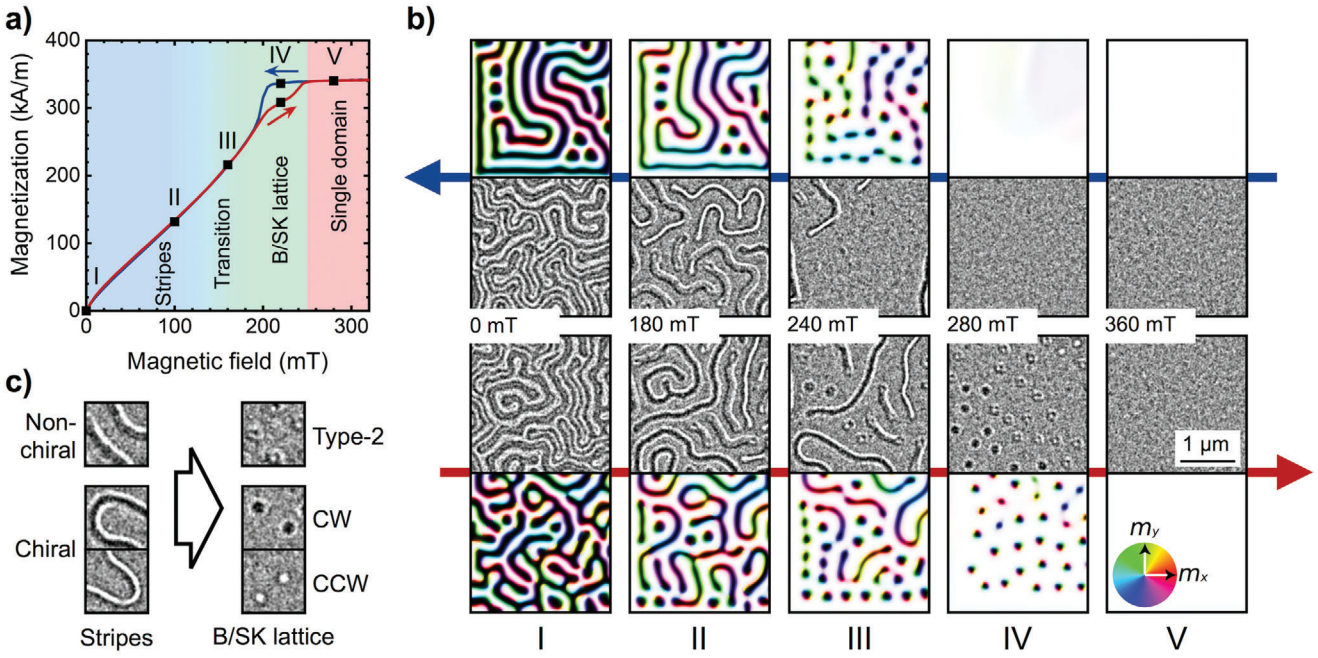

Figure 1. Static magnetic sample properties: a) Out-of-plane *M-H* hysteresis loop of the $[Fe(0.35\ nm)/Gd(0.40\ nm)]_{160}$ thin film at room temperature. Solid lines correspond to *M-H* data for increasing (red) and decreasing (blue) field, black squares mark assignments of LTEM images (I)–(V) in (b) to magnetic field regions in the *M-H* loop. The coloration of magnetic field regimes represent the underlying spin textures. b) LTEM images (grayscale) and micromagnetic simulations (color) of the magnetization for an upsweep (bottom, red arrow) and downsweep (top, blue arrow) of the magnetic field reveal the spin texture corresponding to different magnetic fields (I)-(V) in the hysteresis loop. The direction of *M* in the micromagnetic simulation data is given by the color code. c) Legend of different spin objects indicating the field-induced transformations possible for a magnetic field upsweep with non-chiral and chiral domains walls, type-2 bubbles and clockwise (CW) and counter-clockwise (CCW) skyrmions.

Fe and Gd with composition $[Fe(0.35\ nm)/Gd(0.40\ nm)]_{160}$ deposited on a thermally-oxidized Si(100) substrate. Static magnetic characterization of this sample was performed using Superconducting Quantum Interference Device - Vibrating Sample Magnetometry (SQUID-VSM). Samples deposited on thin commercial Si_3N_4 membranes were used for Lorentz Transmission Electron Microscopy (LTEM) studies to image the static magnetic texture in applied out-of-plane (oop) magnetic fields.

Figure 1a shows the *M-H* hysteresis loop from SQUID-VSM for positive magnetic fields and Figure 1b displays the corresponding LTEM images (gray-scaled middle panels) for representative field values together with micromagnetic simulations of the field-dependent magnetic texture (color-scaled top and bottom panels). Without applied field (Figure 1a,b, left), the sample is in a demagnetized state, and the magnetic texture consists solely of oop stripe domains with Bloch domain walls (region I). We find two different types of domain walls, similar to previous studies:[22,23] Narrow stripes with domain walls that do not exhibit any chirality, and broader stripes with twice the periodicity featuring the same chirality. Applying an increasing oop magnetic field (Figure 1a, red part of *M-H* loop), the oop magnetization of the sample initially increases linearly with the applied magnetic field. In LTEM, this process is visible as a decrease of the density of domain walls (Figure 1b, II, bottom images) and the nucleation of cylindrical spin objects from collapsed narrow stripe domains (so called type-2 magnetic bubbles). For higher magnetic fields (region III), dipolar Bloch-type skyrmions start to nucleate from the broad stripes. In region IV, in a field range of $\mu_0 H \approx 190 - 250$ mT, a bubble and skyrmion (B/SK) lattice with characteristic spacing and groups of spin objects of the same type is formed. Close to saturation, the bubbles vanish and only skyrmions remain (see Figure S4, Supporting Information). For even higher applied fields (region V) magnetic saturation is achieved. Decreasing the magnetic field from saturation does not lead to the appearance of a B/SK lattice in region IV, as reflected in the LTEM images (Figure 1b, IV, top) and *M-H* loop (Figure 1a, blue line) and corroborated by the micromagnetic simulation. The measured oop magnetization in this region is larger than for the upsweep of the magnetic field, as no cylindrical spin objects reducing the oop magnetization exist. The small hysteresis between the increasing (red) and decreasing (blue) *M*(*H*) signal visible in Figure 1a, region IV is thus indicative of the disordered B/SK lattice. For further decreasing field strengths (regions III to I), the evolution of the magnetic texture is again comparable to the upsweep, except that, at least in region III, the initial domain wall density is lower in the decreasing field case. Please note that small differences observed in the magnetic sample properties between SQUID-VSM and LTEM measurements, i.e., higher magnetic field values for the same spin texture in LTEM, arise from the fact that two different substrates are used for the sample preparation resulting in different growth conditions of the films. Micromagnetic simulations match the magnetic field values of the corresponding SQUID-VSM data and are discussed further below.

© 2024 The Authors. Advanced Functional Materials published by Wiley-VCH GmbH

16163028, 0, Downloaded from https://onlinelibrary.wiley.com/doi/10.1002/adfm.202313619 by Max-Planck-Institut fur Multidisziplinare Naturwissenschaften, Wiley Online Library on [02/04/2024]. See the Terms and Conditions (https://onlinelibrary.wiley.com/terms-and-conditions) on Wiley Online Library for rules of use; OA articles are governed by the applicable Creative Commons License

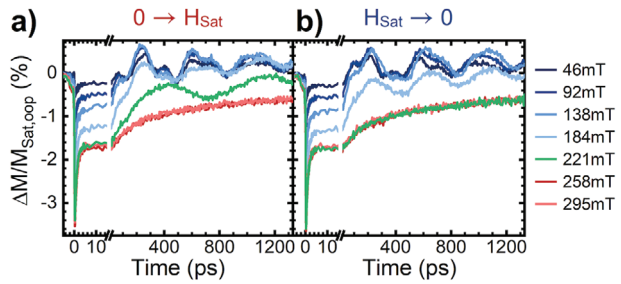

Figure 2. Out-of-plane magnetization dynamics for a weak perturbation in dependence of the applied oop magnetic field: Magnetization dynamics for (a) upsweep and (b) downsweep of the magnetic field. The colors of the curves represent the regions of different spin texture as given in Figure 1a: Stripe domains (blue), B/SK lattice (green), and magnetic saturation (red). Data is normalized to the Kerr signal in magnetic saturation in oop direction.

2.2. Coherent Spin Dynamics in Response to Weak Optical Excitation

After the thorough characterization of the ground state magnetic spin textures, we now focus on the magnetic response of the sample to an ultrashort optical excitation. In particular, we seek correlations between the temporal response and the different spatial textures in Figure 1. For these measurements, we use a comparably weak perturbation (fluence $F = 300$ μJ cm^{-2}, pulse duration $\tau_p < 40$ fs) leading to a total demagnetization of the sample by only 3.5%. Magnetization dynamics $M(t)$ were detected by changes in the light polarization upon reflection of the sample using the magneto-optical Kerr effect (MOKE) in polar geometry with the magnetic field applied in oop direction. For details see the Experimental Section.

Figure 2 depicts the magnetization dynamics in response to the optical excitation and in dependence of the applied oop magnetic field for both an upsweep (Figure 2a) and a downsweep of the magnetic field (Figure 2b). Four processes can be identified: Immediately after photoexcitation, the magnetization is quenched on a timescale of only 300 femtoseconds (fs). This ultrafast demagnetization process is followed by a fast remagnetization on a few picosecond (ps) timescale. During the remagnetization, about half of the initial magnetization is recovered, and the magnetization stays constant thereafter for up to ≈40 ps depending on the applied magnetic field. Finally, the magnetization recovers on a nanosecond (ns)-timescale by thermal transport out of the film. Most notably, in addition to this well-known and incoherent magnetic response,[24,25] a coherent oscillatory signal component is clearly visible in the stripe domain phase (blue transients) and the B/SK lattice phase for the upsweep of the magnetic field (green transient).

The main question now is to what extent this coherent response is indicative of the specific spin texture in the Fe/Gd sample, as given by regions I–V in Figure 1. To answer this question, we performed micromagnetic simulations of the spin dynamics after a magnetization quench of less than 10% (see Experimental Section). **Figure 3** depicts a full comparison of the experimentally found and simulated coherent oscillatory signal components after subtraction of the incoherent background for both the upsweep (Figure 3a) and downsweep (Figure 3c) of the magnetic field. The corresponding Fourier transforms for experiment and micromagnetic simulation are shown in Figure 3b,d, respectively. Note, that the time-axis of the simulation data is shifted by $t_{exc} = 260$ ps with respect to the experimental data, as the spin dynamics in the simulation are not induced by a strong nonequilibrium excitation like in the experiment and the initial change in magnetization or spin object size triggering the breathing evolves on a slower timescale. For details we refer to the Experimental Section.

Evidently, the observed coherent spin dynamics in experiment and simulation match well and show a clear correspondence to the underlying spin textures. The Fourier spectra for magnetic fields of $\mu_0 H = 0 - 190$ mT, i.e., the stripe domain state, show a strong oscillatory mode m_1 with $f_1 \approx 2.3$ GHz, which is identified as a breathing mode of stripe domains in the micromagnetic simulation. A much weaker high-frequency component m_2 with $f_2 \approx 5.4$ GHz is additionally observed in the experiment, however, its origin needs to be further investigated. For magnetic fields of $\mu_0 H \approx 190 - 240$ mT the disordered B/SK lattice is present in the upsweep of the magnetic field only. Correspondingly, experiment and simulation show only in this case an oscillatory mode m_{bsk} with $f_{bsk} \approx 1.4$ GHz. This frequency is identified as a breathing mode of bubbles and skyrmions[26] in the micromagnetic simulation in very good agreement with previous studies on skyrmion dynamics.[14,16,27] We note that micromagnetic simulations predict a slightly lower frequency for magnetic bubbles compared to skyrmions, which occur simultaneously in most of the magnetic field range of region IV in Figure 1a. However, we cannot resolve this difference with our experimental frequency resolution. Last, in saturation, no oscillatory spin dynamics are observed in experiment and simulation.

While the agreement between experiment and simulation is very good in general, we note that small differences do exist in the magnetic field range of $\mu_0 H \approx 150 - 200$ mT for both field up- and downsweep. Here, a transition region appears in the simulation between the stripe and B/SK phase, which does, however, not indicate a true B/SK phase in region IV in the field downsweep in the simulation. Furthermore, there is an apparent phase shift in the oscillatory dynamics with magnetic field in both experiment and simulation. For details on these observations we refer to the Supporting Information.

2.3. Magnetic Phase Transformation in Response to a Strong Optical Excitation

Having shown a clear correlation between spin texture and spin dynamics, we now focus on the response of the spin texture to a strong non-equilibrium excitation of the spin system. We repeat the experiments from above for a strong laser excitation of $F = 3$ mJ cm^{-2}, i.e., an order of magnitude larger fluence than before, and we find significant changes in the observed dynamics. A much stronger incoherent demagnetization of about 45% occurs, i.e., the initial magnetic spin texture is strongly disturbed (see Figure S6a,b, Supporting Information). For a detailed investigation, we again subtracted the incoherent background (**Figure 4**a,b) and performed a Fourier transform (Figure 4c,d).

We now observe the stripe domain phase mode m_1 in a magnetic field range $\mu_0 H = 0 - 100$ mT with slightly lower

© 2024 The Authors. Advanced Functional Materials published by Wiley-VCH GmbH

16163028, 0, Downloaded from https://onlinelibrary.wiley.com/doi/10.1002/adfm.202313619 by Max-Planck-Institut fur Multidisziplinare Naturwissenschaften, Wiley Online Library on [02/04/2024]. See the Terms and Conditions (https://onlinelibrary.wiley.com/terms-and-conditions) on Wiley Online Library for rules of use; OA articles are governed by the applicable Creative Commons License

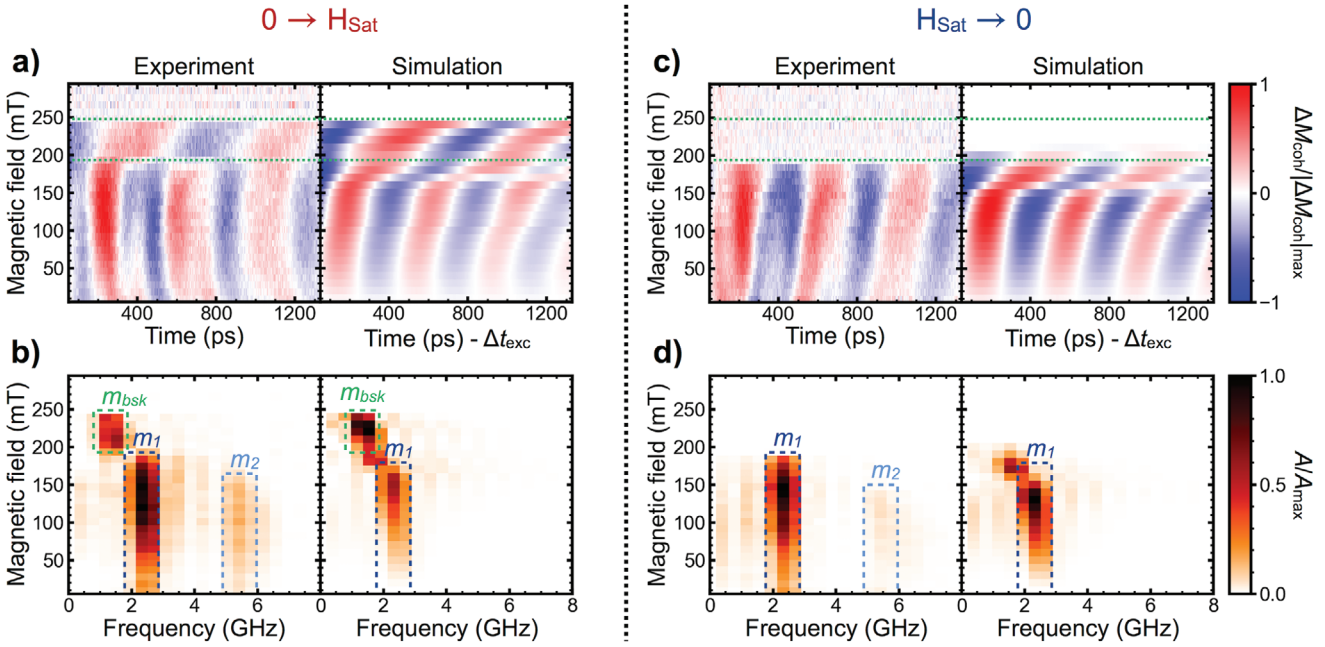

Figure 3. Coherent magnetization dynamics in the experiment and micromagnetic simulation in dependence of the applied oop magnetic field: Coherent magnetization dynamics $\Delta M_{coh}/|\Delta M_{coh}|_{max}$ for (a) upsweep and (c) downsweep of the magnetic field with the corresponding Fourier spectra A/A_{max} (b) and (d), respectively, where identified resonances are marked by dashed boxes. In case of the upsweep (a, b) a unique spin wave mode is observed for the range $\mu_0 H = 190 - 240$ mT marked by the green dashed lines. The time axes of the simulation data are shifted by $\Delta t_{exc} = 260$ ps compared to the experimental time zero. The color scales for each subfigure are normalized to their respective maximum signal value. For details see text.

frequency than before. A second, higher-frequency mode m_2 is weakly present at $f_2 \approx 4.8$ GHz. In contrast to the weak perturbation limit, the mode previously identified to be B/SK breathing now exhibits a clear frequency dependence, shifting from $f \approx 1.4$ GHz at $\mu_0 H \approx 100$ mT to $f \approx 1.0$ GHz at $\mu_0 H \approx 190$ mT. We assign two modes to this magnetic field range: m_{mix} for $\mu_0 H \approx 100 - 150$ mT and m_{bsk} for $\mu_0 H \approx 150 - 190$ mT, which will be discussed further below. Above $\mu_0 H = 190$ mT no oscillatory behavior is observed anymore. Most surprisingly, we now observe the m_{bsk} mode even in the downsweep of the magnetic field (Figure 4b,d), where it was previously absent. This observation suggests that the strong laser excitation itself might induce a B/SK lattice phase in the material. Indeed, skyrmion nucleation from a saturated state by strong laser excitation was recently theoretically predicted[28] and experimentally observed,[19,20] which could explain our findings. However, our micromagnetic simulations strongly suggest that a nucleation of skyrmions from saturation does not appear to be possible for the Fe/Gd multilayers studied here.

To understand the observed behavior better, we performed LTEM measurements before and after femtosecond laser excitation. These measurements indeed allow us to identify the changes in dynamics from Figure 3 to Figure 4 as a laser-induced transformation of the underlying spin texture. We will show in the following that this transformation is not trivial, and not dominantly given by a simple static laser-induced temperature shift of phase stability ranges[22] together with laser-induced skyrmion nucleation from magnetic saturation.[19,20,28]

Upon ultrafast and strong laser excitation, we distinguish five scenarios depending on the field-dependent magnetic ground state of the system depicted in **Figure 5** starting with the upsweep of the magnetic field: A) For low magnetic fields, a pristine stripe domain phase remains nearly unchanged after laser excitation. B) A former mixed stripe domain and B/SK state is turned into a pure B/SK lattice phase, as also observed in the simulation, see Figure S10 (Supporting Information). C) Starting within the B/SK lattice phase, bubbles and skyrmions are annihilated by the laser excitation, i.e., the system is driven into a fully saturated state even by a single laser shot. Thereafter, the new saturated magnetic state is not modified by further laser excitation. D) From saturation, we did not observe any laser-induced creation of skyrmions without irreversibly changing the sample properties, which is in contrast to literature.[19,20,28] However, this observation concurs with the micromagnetic simulations, where it was also not possible to nucleate skyrmions from a saturated spin state. Note that close to saturation in the downsweep of the magnetic field, a gradual transformation of the system starting from a single isolated stripe domain appears possible (see Figure S7, Supporting Information). E) For the downsweep, a plain stripe domain phase with low stripe density is transformed into a mixed phase. Here, all stripe domains convert into cylindrical spin textures after exposure to a single laser pulse and new stripe domains nucleate in regions that are initially saturated (see Figure S9, Supporting Information). Upon subsequent laser excitation the newly generated domains transform into B/SKs. Hence, using ultrafast and strong laser excitation, a pure B/SK lattice phase can be created. A schematic phase diagram of the magnetic texture depending on magnetic field and the number of incident laser pulses can be found in Figure S8 (Supporting Information).

© 2024 The Authors. Advanced Functional Materials published by Wiley-VCH GmbH

16163028, 0, Downloaded from https://onlinelibrary.wiley.com/doi/10.1002/adfm.202313619 by Max-Planck-Institut fur Multidisziplinare Naturwissenschaften, Wiley Online Library on [02/04/2024]. See the Terms and Conditions (https://onlinelibrary.wiley.com/terms-and-conditions) on Wiley Online Library for rules of use; OA articles are governed by the applicable Creative Commons License

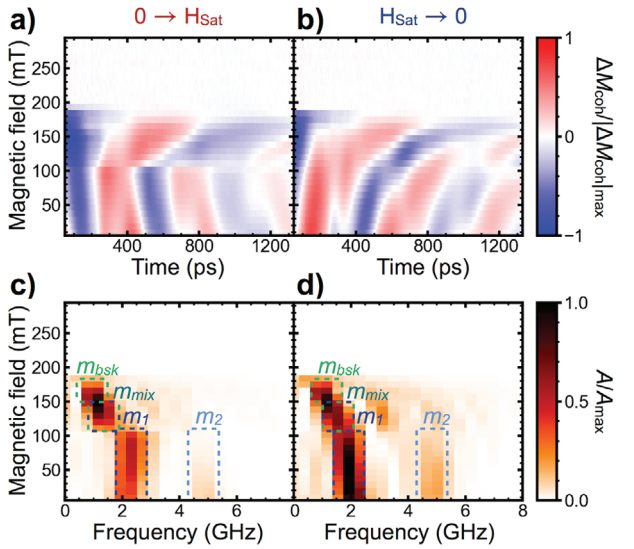

Figure 4. High-fluence coherent magnetization dynamics in time-resolved MOKE in dependence of the applied oop magnetic field: Coherent magnetization dynamics for (a) upsweep and (b) downsweep of the magnetic field with the corresponding Fourier spectrum (c) and (d), respectively. For both directions of magnetic field sweep a shift in spin wave mode is now observed within $\mu_0 H = 100 - 190$ mT. The color scales for each subfigure are normalized to their respective maximum signal value. For details see text.

In comparison to literature, for a Co/Pt multilayer sample, Gerlinger and coworkers[29] observed laser-induced skyrmion nucleation from both i) magnetic saturation and ii) the stripe domain phase. Furthermore, they observed iii) an annihilation of skyrmions and stripe domains close to saturation. In our study, we obviously find similar evidence for processes ii) and iii), but not for i), the laser-induced nucleation from saturation.

However, taking the predictions from micromagnetic simulations and the observations from the LTEM measurements into account, we can now understand the changes in the coherent oscillatory component that come along with the strong excitation in Figure 4: In the upsweep of the magnetic field, the former B/SK lattice phase completely vanishes before the actual data recording starts due to continuous excitation by laser pulses in the time-resolved MOKE experiment. Hence, we observe no oscillatory component, but a signal corresponding to magnetic saturation in the magnetic field range $190 < \mu_0 H < 250$ mT (scenario C, Figure 5). Within $100 < \mu_0 H < 190$ mT we observe mode frequencies previously attributed to a pure B/SK phase, but now exhibiting a frequency downshift with magnetic field. Here, two phases are present, m_{bsk} and m_{mix}. For $150 < \mu_0 H < 190$ mT (scenario B, Figure 5), the initially mixed stripe domain and B/SK phase is laser-transformed into a pure B/SK lattice phase, leading to the low-frequency m_{bsk} mode at $f_{bsk} \approx 1.0$ Ghz. The slightly higher frequency mode m_{mix} at $f_{mix} \approx 1.4$ Ghz observed in Figure 4c for magnetic fields of about $110 < \mu_0 H < 150$ mT originates from a mixed phase that forms upon laser excitation out of a pristine stripe domain phase exhibiting none or only very few skyrmions, respectively. This means that no final pure B/SK lattice phase is created within this field range (see also Figure S5, Supporting Information). In the downsweep of the magnetic field, for high fields ($150 < \mu_0 H < 190$ mT) a pure B/SK lattice phase is formed out of a pure stripe phase (scenario E, Figure 5), and, for lower fields ($100 < \mu_0 H < 150$ mT), a mixed phase is the final state. For fields below 100 mT, stripe domain mode m_1 at $f_1 \approx 1.9 - 2.3$ GHz is dominant for both field up- and downsweep. All these mechanisms lead to the generally more equal oscillatory behavior observed for the strong perturbation case for magnetic field up- and downsweep. However, the absence of an initially mixed phase in the downsweep hinders the generation of a B/SK lattice phase. For equal magnetic fields we observe less bubbles and skyrmions being created in the downsweep of the magnetic field, resulting in a dominance of the stripe's oscillatory component in the generated mixed phase. Finally, the generally lower frequencies of all modes can most likely be attributed to the stronger transient laser-induced change of macroscopic sample properties, e.g., sample temperature, magnetization and anisotropies.[22] Redshifting of skyrmion frequencies has also been observed in Refs. [17,26] with increasing excitation strength or sample temperature.

Closing the discussion, three further points are noteworthy: First, an asymmetry in the observed coherent spin system response exists for the upsweep and downsweep of the magnetic field in the field regions assigned to the stripe domain phase. This asymmetry increases with a stronger perturbation. This is evident from the different shifts of magnetic oscillations for the upsweep and downsweep of the magnetic field in Figure 3a,c as well as Figure 4a,b, which even shows a frequency shift between the up and down field sweeps (cf. Figure 4c,d). However, SQUID-VSM and LTEM data from Figure 1 do not suggest any specific macroscopic difference in the low-field range for both field sweep directions, except possibly in domain wall density. Currently, we do not have an explanation for this behavior, but aim to investigate this further in the future. Second, in contrast to Refs. [19,20,29], skyrmion creation in our case is only possible if there is an initially existing chiral spin texture. Even further, the nucleation of skyrmions does not only have a lower but also an upper fluence threshold. Above a certain fluence, a mixed phase is formed in the region of maximum excitation that is surrounded by a pure skyrmion phase due to the Gaussian intensity distribution of the laser pulse, see Figure S12 (Supporting Information). Last, we want to note that no influence of spin texture on the incoherent magnetization dynamics was observed, neither on the sub-ps timescale nor during the remagnetization.

3. Conclusion

In summary, we studied the response of the spin-textured material Fe/Gd to weak and strong ultrafast laser excitation. In the weak excitation limit, unique coherent spin dynamics evolve that allowed us to directly identify the magnetic stripe domain phase, the bubble/skyrmion lattice phase, as well as magnetic saturation. In the strong excitation limit, we observed significant changes in the dynamic magnetic phase diagram, which we attributed to a laser-induced transformation of the spin texture as verified by micromagnetics and LTEM measurements. Indeed, from the stripe domain state, we created both a bubble/skyrmion lattice and a mixed phase of bubbles, skyrmions, and stripe domains, depending on the external magnetic field. These results highlight that optical control of spin wave resonances is

© 2024 The Authors. Advanced Functional Materials published by Wiley-VCH GmbH

16163028, 0, Downloaded from https://onlinelibrary.wiley.com/doi/10.1002/adfm.202313619 by Max-Planck-Institut fur Multidisziplinare Naturwissenschaften, Wiley Online Library on [02/04/2024]. See the Terms and Conditions (https://onlinelibrary.wiley.com/terms-and-conditions) on Wiley Online Library for rules of use; OA articles are governed by the applicable Creative Commons License

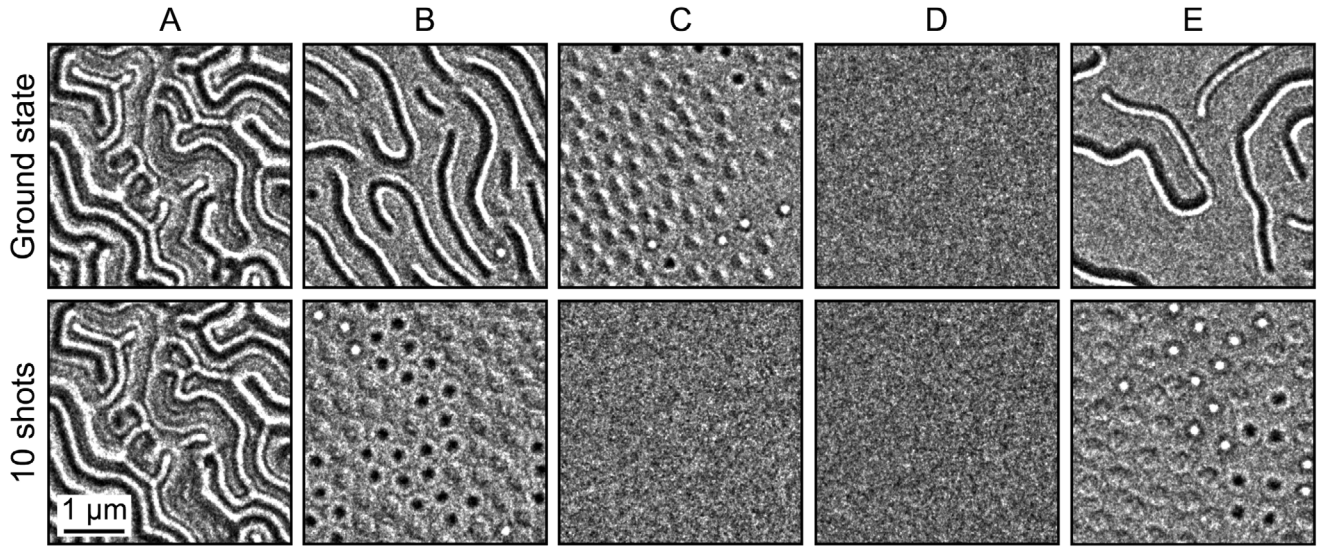

Figure 5. Laser-induced transformation of magnetic textures in LTEM: LTEM experimental data showing the magnetic texture before and after strong laser excitation of $F = 6.4$ mJ cm^{-2}. A) Unmodified stripe domain phase for low magnetic fields; B) transformation of a mixed phase into a B/SK lattice phase; C) annihilation of bubbles and skyrmions; D) unmodified saturated magnetic state; E) transformation of a stripe state in the downsweep of the magnetic field into a mixed state (see Figure S9, Supporting Information) and then further into a B/SK lattice state.

possible by optical transformation of the spin textures in the material. Moreover, these rich spin physics are observed at room temperature and at quite moderate magnetic fields and laser fluence, making the Fe/Gd multilayer system an attractive model system for fundamental studies of spin texture-based physics, as well as potential application in spin-electronics in the future.

4. Experimental Section

Sample Preparation and Static Characterization: [Fe(0.35 nm)/Gd(0.40 nm)]$_{160}$ multilayer samples were prepared on both thermally-oxidized Si(100) substrates for SQUID-VSM and TR-MOKE measurements, as well as on 30-nm-thick Si_3N_4 membranes required for LTEM imaging. The films were deposited at room temperature by dc magnetron sputtering in one run. Nevertheless, slightly varying magnetic properties were obtained due to different growth conditions during deposition on the two different substrates. The sputter process was carried out using an Ar working pressure of 3.5 µbar in an ultra-high vacuum chamber. For all samples, a 5-nm-thick Pt seed layer and a 5-nm-thick Si_3N_4 capping layer were used to protect the films from oxidation. The thickness of the layers was controlled by a calibrated quartz balance during layer deposition.

The magnetic properties of the samples were analyzed by SQUID-VSM. *M-H* hysteresis loops were measured both in out-of-plane and in-plane configuration at room temperature (see Figure S13, Supporting Information). The magnetic spin textures were imaged by LTEM at room temperature using a JEOL NEOARM-200F system operated at 200 keV beam energy in the Fresnel mode with an underfocus of 2 mm. Images were recorded with a Gatan OneView camera in external out-of-plane magnetic fields.

Time-Resolved Magneto-Optical Kerr Effect (TR-MOKE): Transient reflectivity $\Delta R(t)$ and magnetization dynamics $\Delta M(t)$ were measured simultaneously using a bichromatic pump-probe setup on an [Fe(0.35 nm)/Gd(0.40 nm)]$_{160}$ multilayer stack deposited on a thermally-oxidized Si(100) substrate. Sub-ps laser pulses were generated by a fiber amplifier system operating at a repetition rate of 50 kHz. A pulse duration of less than 40 fs was achieved at the sample position via spectral broadening in a gas-filled hollow core fiber and subsequent compression with chirped mirrors.[30] In the setup, the fundamental light pulses with central wavelength of 1030 nm and their second harmonic at 515 nm were used as pump and probe pulses, respectively. External out-of-plane magnetic fields up to $\mu_0 H = 0.7$ T could be applied by mounting the sample in-between the poles of a variable-gap electromagnet. The data was measured by a balanced bridge detector and collected by a 250 MHz digitizer card enabling single pulse detection. Using a mechanical chopper to improve signal quality, both the pumped and the unpumped signals could be recorded, allowing for maximum scope of data post processing. Data was acquired in polar Kerr geometry, where the magnetic field was applied in oop direction. All $M(t)$ data shown were recorded as the difference of $M(t)$ traces for two opposite magnetic fields to remove nonmagnetic signal components, taking care to set the correct spin texture by approaching the current magnetic field either from below or above.

Lorentz Transmission Electron Microscopy with In Situ Optical Excitation: To obtain a better understanding of the spin dynamics observed in TR-MOKE in the strong excitation limit, a sample on a thin commercial Si_3N_4 membrane was studied by LTEM at the Göttingen Ultrafast Transmission Electron Microscope, allowing for in situ optical excitation.[18,31,32] Energy-filtered images were recorded by using a CEOS CEFID equipped with a TVIPS XF416 at a 10 eV window-width, an acceleration voltage of 200 keV and a 6 mm defocus. In these experiments a laser source with a wavelength of 750 nm and a pulse width of around 300 fs excites the sample under a near normal angle of incidence with a defined number of laser pulses starting from single shot. At various oop magnetic fields, micrographs were acquired before, after a single and after multiple excitations to observe changes of the samples magnetic texture. In order to obtain reproducible magnetic textures before laser excitation, the sample was fully saturated with an oop field before approaching a specific field magnitude.

In addition to the somewhat different laser conditions, the LTEM sample on the thin TEM membrane had different thermal couplings and strain compared to the MOKE sample on the rigid Si substrate. This also leads to slightly higher magnetic field ranges, where the stripe phase, B/SK lattice phase, and magnetic saturation were present. Due to these differences in experimental conditions, a quantitative fluence matching between TR-MOKE and LTEM experiments was not attempted. However, the LTEM results, at a fluence about a factor of two higher than in TR-MOKE, allow to fully understand the changes to the magnetic texture by laser excitation and allow to perfectly explain the observations in the TR-MOKE measurements. To obtain the fluences in the LTEM measurements from the laser pulse energy, a $1/e^2$ beam diameter of 60 µm was used,

© 2024 The Authors. Advanced Functional Materials published by Wiley-VCH GmbH

16163028, 0, Downloaded from https://onlinelibrary.wiley.com/doi/10.1002/adfm.202313619 by Max-Planck-Institut fur Multidisziplinare Naturwissenschaften, Wiley Online Library on [02/04/2024]. See the Terms and Conditions (https://onlinelibrary.wiley.com/terms-and-conditions) on Wiley Online Library for rules of use; OA articles are governed by the applicable Creative Commons License

16163028, 0, Downloaded from https://onlinelibrary.wiley.com/doi/10.1002/adfm.202313619 by Max-Planck-Institut fur Multidisziplinare Naturwissenschaften, Wiley Online Library on [02/04/2024]. See the Terms and Conditions (https://onlinelibrary.wiley.com/terms-and-conditions) on Wiley Online Library for rules of use; OA articles are governed by the applicable Creative Commons License

estimated from the maximum region of switched magnetic texture upon laser excitation.

Static Micromagnetic Simulations: magnum.np was used,[33] a GPU-enhanced micromagnetic simulation software, to perform large-scale micromagnetic simulations. The Fe/Gd multilayers were simulated as a 3D ferromagnet with low saturation magnetization $M_s = 340$ kA m^{-1} and low perpendicular magnetic anisotropy $K_u = 40$ kJ m^{-3}. The exchange constant was chosen $A_{ex} = 6$ pJ m^{-1}. Our finite-difference micromagnetic solver discretizes the simulation box into $512 \times 512 \times 10$ cuboids, each with a constant volume of $10 \times 10 \times 11.2$ nm^3. Note that all simulations were performed without any thermal fluctuations. Basically, the system was simulated at $T = 0$K, but with effective magnetic parameters that were measured at room temperature. Similar modeling was used in experimental studies on Fe/Gd-based multilayers.[22,23] To obtain the *M-H* hysteresis loops shown in Figure 1, the simulation was started from a cellwise random magnetization state. The structure in zero field was relaxed by solving the Landau-Lifshitz-Gilbert (LLG) equation numerically[34] at high damping $\alpha = 1.0$, where the demagnetization, exchange, anisotropy and Zeeman energies were included in the calculation of the effective field. The stripe domain structure was obtained as the new initial state. Once the magnetic system was relaxed with respect to its energy, an oop field along the *z*-direction was applied. The magnetic field was increased by 2 mT after each relaxation step in which the LLG was solved for 10 ns. The complete hysteresis was then simulated by raising and lowering the field between ± 250 mT. Magnetization states at each field were saved to be used as input for dynamic simulations to simulate the resonance of the spin objects.

Dynamic Micromagnetic Simulations: The intrinsic response of the spin textures was simulated with the magnetization states obtained from the static simulations. Commonly, ultrafast laser demagnetization can be described micromagnetically by including a stochastic temperature-dependent term to the LLG, where the temperature in the magnetic system is calculated from the excitation energy via the two-temperature model.[35] However, the demagnetization process itself was not of interest in this study, but rather the excitation of the magnetic system and how this relaxes into its equilibrium state. Thus, a similar approach was employed as for simulating ferromagnetic resonance (FMR).[36] That is, it was assumed that the laser pulse heats up the system and alters the temperature-dependent magnetic parameters. Excitation of the system was then regarded as the attempt of the magnetization to try to return to its original energetic minimum. Consider the base magnetic parameters $M_S = 340$ kA m^{-1}, $K_U = 40$ kJ m^{-3}, and $A_{ex} = 6$ pJ m^{-1} at room temperature. For a given excitation $E = 0.05 - 0.25$, $M_{S,\,exc} = (1 - E) \times M_S$. $K_{U,\,exc}$ scales with $K_U \times (M_{S,\,exc}/M_S)^2$, and $A_{Ex,\,exc}$ scales with $A_{Ex} \times (M_{S,\,exc}/M_S)^2$.[37] The magnetization states from the zero-temperature hysteresis at a defined field were used as starting points. The LLG equation was solved for 1ns at moderate damping $\alpha = 0.1$ to get the magnetization near its new energetic minimum for the new set of magnetic parameters ($M_{S,\,exc}$, $K_{U,\,exc}$, $A_{Ex,\,exc}$). The initial magnetic parameters (M_S, K_U, A_{Ex}) were set and the damping was reduced to $\alpha = 0.02$. The simulation time was 10 ns. The magnetization starts to oscillate back into the original or new ground state, based on the strength of the excitation. Total resonances were then captured by first recording the averaged magnetization components for every $\Delta t = 1$ ps and performing an FFT. To probe the influence of a stroboscopic measurement technique, the excitation was repeated up to ten times and the magnetization state was recorded after each excitation, where changes in the magnetization states could be observed for high excitation amplitudes. The resonance frequencies of the stripe domain, bubble and the skyrmion were separated by averaging the magnetization in a smaller simulation box. For the bubble/skyrmion phase m_z was averaged for a single bubble/skyrmion and recorded for each time step $\Delta t = 10$ ps. For the stripe domain, first an appropriately small section was found where only one stripe domain was stable and had almost parallel domain walls. The magnetization along a line 500 nm long was then sampled. The magnetization was then averaged for each component at the same time step as used for the skyrmions.

Subtraction of Incoherent Background: From Figure 2 and Figure S6 (Supporting Information) it is evident that the coherent dynamics are superimposed by incoherent dynamics stemming from the process of magnetization recovery. Here, the routine is presented which was used to subtract the incoherent background from the experimental data.

In case of high magnetic fields ($\mu_0 H > 200$ mT) the sample was in a single domain state and no coherent oscillation was observed. To account for slight changes between measurements, the average of the four curves with highest applied fields ($\mu_0 H = 320, 370, 460, 550$ mT) was taken after normalizing them to their respective minimum magnetization. A bi-exponential function $A\exp(-t/\tau_1) + B\exp(-t/\tau_2)$ was fitted to this mean curve to obtain a noise-free background function $f_{bg}(t)$. Then, for each field-dependent transient magnetization curve $\Delta M(t)$ the background function scaled to the respective minimum magnetization, i.e., $\Delta M(t)_{coh} = \Delta M(t) - \min[\Delta M(t)] \cdot f_{bg}(t)$, was subtracted to take the field-dependent projection of M on M_{oop} into account. This procedure removed any time-dependent incoherent background, i.e., the time constants of remagnetization did not depend on the applied magnetic field. Last, a field-dependent offset constant was removed to center the remaining oscillation around zero.

Supporting Information

Supporting Information is available from the Wiley Online Library or from the author.

Acknowledgements

S.K. and C.A. gratefully acknowledge the Austrian Science Fund (FWF) for support through Grant no. P34671 (Vladimir). S.K. and D.Su. acknowledge the Austrian Science Fund (FWF) for support through Grant no. I 6267 (CHIRALSPIN). T.S. and M.A. gratefully acknowledge funding from Deutsche Forschungsgemeinschaft (DFG, German Research Foundation) grant no. 507821284. D.St., S.M. and T.T. acknowledge funding by the DFG, grant no. 217133147/SFB 1073, project A02. The computational results presented have been achieved in part using the Vienna Scientific Cluster (VSC).

Open access Publication Funds of the Göttingen University enabled and organized by Projekt DEAL.

Conflict of Interest

The authors declare no conflict of interest.

Data Availability Statement

The data that support the findings of this study are available from the corresponding author upon reasonable request.

Keywords

breathing mode, dipolar stabilized bubble/skyrmion lattice, ferromagnetism, laser-induced nucleation/annihilation of spin texture, magnetic materials, spintronics, topology

Received: November 1, 2023
Revised: February 23, 2024
Published online:

[1] G. Finocchio, F. Büttner, R. Tomasello, M. Carpentieri, M. Kläui, *J. Phys. D: Appl. Phys.* **2016**, *49*, 423001.

© 2024 The Authors. Advanced Functional Materials published by Wiley-VCH GmbH

[2] A. Fert, N. Reyren, V. Cros, *Nat. Rev. Mater.* **2017**, *2*, 1.
[3] D. Prychynenko, M. Sitte, K. Litzius, B. Krüger, G. Bourianoff, M. Kläui, J. Sinova, K. Everschor-Sitte, *Phys. Rev. Appl.* **2018**, *9*, 014034.
[4] K. M. Song, J.-S. Jeong, B. Pan, X. Zhang, J. Xia, S. Cha, T.-E. Park, K. Kim, S. Finizio, J. Raabe, J. Chang, Y. Zhou, W. Zhao, W. Kang, H. Ju, S. Woo, *Nat. Electron.* **2020**, *3*, 148.
[5] X. Zhang, Y. Zhou, K. M. Song, T.-E. Park, J. Xia, M. Ezawa, X. Liu, W. Zhao, G. Zhao, S. Woo, *J. Phys.: Condens. Matter* **2020**, *32*, 143001.
[6] A. V. Chumak, P. Kabos, M. Wu, C. Abert, C. Adelmann, A. O. Adeyeye, J. Åkerman, F. G. Aliev, A. Anane, A. Awad, C. H. Back, A. Barman, G. E. W. Bauer, M. Becherer, E. N. Beginin, V. A. S. V. Bittencourt, Y. M. Blanter, P. Bortolotti, I. Boventer, D. A. Bozhko, S. A. Bunyaev, J. J. Carmiggelt, R. R. Cheenikundil, F. Ciubotaru, S. Cotofana, G. Csaba, O. V. Dobrovolskiy, C. Dubs, M. Elyasi, K. G. Fripp, et al., *IEEE Trans. Magn.* **2022**, *58*, 1.
[7] M. Hassan, S. Koraltan, A. Ullrich, F. Bruckner, R. O. Serha, K. V. Levchenko, G. Varvaro, N. S. Kiselev, M. Heigl, C. Abert, D. Suess, M. Albrecht, *Nat. Phys.* **2024**, https://doi.org/10.1038/s41567-023-02358-z.
[8] A. Bogdanov, A. Hubert, *J. Magn. Magn. Mater.* **1994**, *138*, 255.
[9] U. K. Roessler, A. Bogdanov, C. Pfleiderer, *Nature* **2006**, *442*, 797.
[10] X. Yu, Y. Onose, N. Kanazawa, J. H. Park, J. Han, Y. Matsui, N. Nagaosa, Y. Tokura, *Nature* **2010**, *465*, 901.
[11] B. Lenk, H. Ulrichs, F. Garbs, M. Münzenberg, *Phys. Rep.* **2011**, *507*, 107.
[12] H. Yu, J. Xiao, H. Schultheiss, *Phys. Rep.* **2021**, *905*, 1.
[13] D. Petti, S. Tacchi, E. Albisetti, *J. Phys. D: Appl. Phys.* **2022**, *55*, 293003.
[14] N. Ogawa, S. Seki, Y. Tokura, *Sci. Rep.* **2015**, *5*, 9552.
[15] P. Padmanabhan, F. Sekiguchi, R. B. Versteeg, E. Slivina, V. Tsurkan, S. Bordács, I. Kézsmárki, P. H. M. van Loosdrecht, *Phys. Rev. Lett.* **2019**, *122*, 107203.
[16] F. Sekiguchi, K. Budzinauskas, P. Padmanabhan, R. B. Versteeg, V. Tsurkan, I. Kézsmárki, F. Foggetti, S. Artyukhin, P. H. M. van Loosdrecht, *Nat. Commun.* **2022**, *13*, 3212.
[17] J. Kalin, S. Sievers, H. Füser, H. W. Schumacher, M. Bieler, F. García-Sánchez, A. Bauer, C. Pfleiderer, *Phys. Rev. B* **2022**, *106*, 054430.
[18] T. Eggebrecht, M. Möller, J. G. Gatzmann, N. Rubiano da Silva, A. Feist, U. Martens, H. Ulrichs, M. Münzenberg, C. Ropers, S. Schäfer, *Phys. Rev. Lett.* **2017**, *118*, 097203.
[19] S.-G. Je, P. Vallobra, T. Srivastava, J.-C. Rojas-Sánchez, T. H. Pham, M. Hehn, G. Malinowski, C. Baraduc, S. Auffret, G. Gaudin, S. Mangin, H. Béa, O. Boulle, *Nano Lett.* **2018**, *18*, 7362.
[20] F. Büttner, B. Pfau, M. Böttcher, M. Schneider, G. Mercurio, C. M. Günther, P. Hessing, C. Klose, A. Wittmann, K. Gerlinger, L.-M. Kern, C. Strüber, C. von Korff Schmising, J. Fuchs, D. Engel, A. Churikova, S. Huang, D. Suzuki, I. Lemesh, M. Huang, L. Caretta, D. Weder, J. H. Gaida, M. Möller, T. R. Harvey, S. Zayko, K. Bagschik, R. Carley, L. Mercadier, J. Schlappa, et al., *Nat. Mater.* **2021**, *20*, 30.
[21] M. Khela, M. Dabrowski, S. Khan, P. S. Keatley, I. Verzhbitskiy, G. Eda, R. J. Hicken, H. Kurebayashi, E. J. G. Santos, *Nat. Commun.* **2023**, *14*, 1378.
[22] S. A. Montoya, S. Couture, J. J. Chess, J. C. T. Lee, N. Kent, D. Henze, S. K. Sinha, M.-Y. Im, S. D. Kevan, P. Fischer, B. J. McMorran, V. Lomakin, S. Roy, E. E. Fullerton, *Phys. Rev. B* **2017**, *95*, 024415.
[23] M. Heigl, S. Koraltan, M. Vaňatka, R. Kraft, C. Abert, C. Vogler, A. Semisalova, P. Che, A. Ullrich, T. Schmidt, J. Hintermayr, D. Grundler, M. Farle, M. Urbánek, D. Suess, M. Albrecht, *Nat. Commun.* **2021**, *12*, 2611.
[24] E. Beaurepaire, J.-C. Merle, A. Daunois, J.-Y. Bigot, *Phys. Rev. Lett.* **1996**, *76*, 4250.
[25] A. Kirilyuk, A. V. Kimel, T. Rasing, *Rev. Mod. Phys.* **2010**, *82*, 2731.
[26] M. Mochizuki, *Phys. Rev. Lett.* **2012**, *108*, 017601.
[27] Y. Onose, Y. Okamura, S. Seki, S. Ishiwata, Y. Tokura, *Phys. Rev. Lett.* **2012**, *109*, 037603.
[28] W. Koshibae, N. Nagaosa, *Nat. Commun.* **2014**, *5*, 5148.
[29] K. Gerlinger, B. Pfau, F. Büttner, M. Schneider, L.-M. Kern, J. Fuchs, D. Engel, C. M. Günther, M. Huang, I. Lemesh, L. Caretta, A. Churikova, P. Hessing, C. Klose, C. Strüber, C. v. K. Schmising, S. Huang, A. Wittmann, K. Litzius, D. Metternich, R. Battistelli, K. Bagschik, A. Sadovnikov, G. S. D. Beach, S. Eisebitt, *Appl. Phys. Lett.* **2021**, *118*, 192403.
[30] C. Möller, H. Probst, J. Otto, K. Stroh, C. Mahn, S. Steil, V. Moshnyaga, G. S. M. Jansen, D. Steil, S. Mathias, *Rev. Sci. Instrum.* **2021**, *92*, 065107.
[31] A. Feist, N. Bach, N. Rubiano da Silva, T. Danz, M. Möller, K. E. Priebe, T. Domröse, J. G. Gatzmann, S. Rost, J. Schauss, S. Strauch, R. Bormann, M. Sivis, S. Schäfer, C. Ropers, *Ultramicroscopy* **2017**, *176*, 63.
[32] M. Möller, J. H. Gaida, S. Schäfer, C. Ropers, *Commun. Phys.* **2020**, *3*, 36.
[33] F. Bruckner, S. Koraltan, C. Abert, D. Suess, *Sci. Rep.* **2023**, *13*, 12054.
[34] C. Abert, *Eur. Phys. J. B* **2019**, *92*, 120.
[35] U. Atxitia, O. Chubykalo-Fesenko, N. Kazantseva, D. Hinzke, U. Nowak, R. W. Chantrell, *Appl. Phys. Lett.* **2007**, *91*, 232507.
[36] A. Baker, M. Beg, G. Ashton, M. Albert, D. Chernyshenko, W. Wang, S. Zhang, M.-A. Bisotti, M. Franchin, C. L. Hu, R. Stamps, T. Hesjedal, H. Fangohr, *J. Magn. Magn. Mater.* **2017**, *421*, 428.
[37] R. Moreno, R. F. L. Evans, S. Khmelevskyi, M. C. Muñoz, R. W. Chantrell, O. Chubykalo-Fesenko, *Phys. Rev. B* **2016**, *94*, 104433.

© 2024 The Authors. Advanced Functional Materials published by Wiley-VCH GmbH

16163028, 0, Downloaded from https://onlinelibrary.wiley.com/doi/10.1002/adfm.202313619 by Max-Planck-Institut fur Multidisziplinare Naturwissenschaften, Wiley Online Library on [02/04/2024]. See the Terms and Conditions (https://onlinelibrary.wiley.com/terms-and-conditions) on Wiley Online Library for rules of use; OA articles are governed by the applicable Creative Commons License